Measurement of the differential branching fraction of the decay #[superscript 0][subscript b] → #μ[superscript +]μ[superscript −]

Physics Letters B 725 (2013) 25–35

Contents lists available at SciVerse ScienceDirect

Physics Letters B

www.elsevier.com/locate/physletb

Measurement of the differential branching fraction of the decay $\Lambda_b^0 \to \Lambda\mu^+\mu^-$

LHCb Collaboration

ARTICLE INFO

Article history:
Received 11 June 2013
Received in revised form 28 June 2013
Accepted 29 June 2013
Available online 4 July 2013
Editor: W.-D. Schlatter

ABSTRACT

The differential branching fraction of the decay $\Lambda_b^0 \to \Lambda\mu^+\mu^-$ is measured as a function of the square of the dimuon invariant mass, q^2. A yield of 78 ± 12 $\Lambda_b^0 \to \Lambda\mu^+\mu^-$ decays is observed using data, corresponding to an integrated luminosity of 1.0 fb^{-1}, collected by the LHCb experiment at a centre-of-mass energy of 7 TeV. A significant signal is found in the q^2 region above the square of the J/ψ mass, while at lower-q^2 values upper limits are set on the differential branching fraction. Integrating the differential branching fraction over q^2, while excluding the J/ψ and $\psi(2S)$ regions, gives a branching fraction of $\mathcal{B}(\Lambda_b^0 \to \Lambda\mu^+\mu^-) = (0.96 \pm 0.16(\text{stat}) \pm 0.13(\text{syst}) \pm 0.21(\text{norm})) \times 10^{-6}$, where the uncertainties are statistical, systematic and due to the normalisation mode, $\Lambda_b^0 \to J/\psi\Lambda$, respectively.

1. Introduction

The decay $\Lambda_b^0 \to \Lambda\mu^+\mu^-$ is a rare ($b \to s$) flavour-changing neutral current process that in the Standard Model proceeds through electroweak loop (penguin and $W^\pm$ box) diagrams. Since non-Standard Model particles may also participate in these loop diagrams, measurements of this and similar decays can be used to search for physics beyond the Standard Model. In the past, more emphasis has been placed on the study of rare decays of mesons than of baryons, in part due to the theoretical complexity of the latter [1]. In the particular system studied in this Letter, the decay products include only a single hadron, simplifying the theoretical modelling of hadronic physics in the final state.

The study of Λ_b^0 baryon decays is of considerable interest for two reasons. Firstly, as the Λ_b^0 baryon has non-zero spin, there is the potential to improve the limited understanding of the helicity structure of the underlying Hamiltonian, which cannot be extracted from mesonic decays [1,2]. Secondly, as the composition of the Λ_b^0 baryon may be considered as the combination of a heavy quark with a light diquark system, the hadronic physics differs significantly from that of the B meson decay. This may allow this aspect of the theory to be tested, which may lead to improvements in understanding of B mesons.

Theoretical aspects of the $\Lambda_b^0 \to \Lambda\mu^+\mu^-$ decay have been considered both in the SM and in various scenarios of physics beyond the Standard Model [3–15]. Although based on the same effective Hamiltonian as that for the corresponding mesonic transitions, the hadronic form factors for the Λ_b^0 baryon case are less well-known due to the smaller number of experimental constraints. This leads to a large spread in the predicted branching fractions. The differential branching fraction as a function of the square of the dimuon invariant mass, $q^2 \equiv m^2_{\mu^+\mu^-}$, is of particular interest. The approaches taken by the theoretical calculations depend on the q^2 region. By comparing predictions with data as a function of q^2, these different methods of treating form factors are tested.

The first observation of the decay $\Lambda_b^0 \to \Lambda\mu^+\mu^-$ by the CDF Collaboration [16] had a signal yield of 24 ± 5 events, corresponding to an absolute branching fraction $\mathcal{B}(\Lambda_b^0 \to \Lambda\mu^+\mu^-) = (1.73 \pm 0.42(\text{stat}) \pm 0.55(\text{syst})) \times 10^{-6}$, with evidence for signal at q^2 above the square of the mass of the $\psi(2S)$ resonance.

Following previous measurements of rare decays involving dimuon final states [17,18], a first measurement by LHCb of the differential and total branching fractions for the rare decay $\Lambda_b^0 \to \Lambda\mu^+\mu^-$ is reported. The inclusion of charge conjugate modes is implicit throughout. The rates are normalised with respect to the $\Lambda_b^0 \to J/\psi\Lambda$ decay, with $J/\psi \to \mu^+\mu^-$. This analysis uses a pp collision data sample, corresponding to an integrated luminosity of 1.0 fb^{-1}, collected during 2011 at a centre-of-mass energy of 7 TeV.

2. Detector and software

The LHCb detector [19] is a single-arm forward spectrometer covering the pseudorapidity range $2 < \eta < 5$, designed for the study of particles containing b or c quarks. The detector includes a high-precision tracking system consisting of a silicon-strip vertex detector (VELO) surrounding the pp interaction region, a large-area silicon-strip detector located upstream of a dipole magnet with a bending power of about 4 Tm, and three stations of silicon-strip detectors and straw drift tubes placed downstream. The combined

0370-2693/
http://dx.doi.org/10.1016/j.physletb.2013.06.060

tracking system provides a momentum measurement with relative uncertainty that varies from 0.4% at 5 GeV/c to 0.6% at 100 GeV/c, and impact parameter (IP) resolution of 20 μm for tracks with high transverse momentum. Charged hadrons are identified using two ring-imaging Cherenkov detectors [20]. Photon, electron and hadron candidates are identified by a calorimeter system consisting of scintillating-pad and preshower detectors, an electromagnetic calorimeter and a hadronic calorimeter. Muons are identified by a system composed of alternating layers of iron and multiwire proportional chambers [21].

The trigger [22] consists of a hardware stage, based on information from the calorimeter and muon systems, followed by a software stage, which applies a full event reconstruction. Candidate events are first required to pass a hardware trigger which selects muons with a transverse momentum, $p_{\rm T} > 1.48$ GeV/c. In the subsequent software trigger, at least one of the final state particles is required to have both $p_{\rm T} > 0.8$ GeV/c and an impact parameter greater than 100 μm with respect to all of the primary pp interaction vertices (PVs) in the event. Finally, the tracks of two or more of the final state particles are required to form a vertex that is significantly displaced from the PVs in the event.

A candidate $\Lambda_b^0 \to \Lambda\mu^+\mu^-$ or $\Lambda_b^0 \to J/\psi\Lambda$ decay that is directly responsible for triggering both the hardware and software triggers is denoted as "trigger on signal". An event in which a Λ_b^0 baryon is reconstructed in either of these modes but none of the daughter particles are necessary for the trigger decision is referred to as "trigger independent of signal". As these two categories of event are not mutually exclusive, the overlap may be used to estimate the efficiency of the trigger selection directly from data.

In the simulation, pp collisions are generated using Pythia 6.4 [23] with a specific LHCb configuration [24]. Decays of hadronic particles are described by EvtGen [25] in which final state radiation is generated using Photos [26]. The interaction of the generated particles with the detector and its response are implemented using the Geant4 toolkit [27,28] as described in Ref. [29].

3. Candidate selection

Candidate $\Lambda_b^0 \to \Lambda\mu^+\mu^-$ (signal mode) and $\Lambda_b^0 \to J/\psi\Lambda$ (normalisation mode) decays are reconstructed from muon, Λ baryon and J/ψ candidates. The J/ψ candidates are reconstructed via their dimuon decays and therefore the $\Lambda_b^0 \to J/\psi\Lambda$ decay is an ideal normalisation process. The dimuon candidates are formed from two oppositely-charged particles identified as muons [21,20]. Good track quality is ensured by requiring χ^2/ndf (χ^2 per degree of freedom) <4 for a track fit. The candidates must also have $\chi^2_{\rm IP}$ with respect to any primary interaction greater than 16, where $\chi^2_{\rm IP}$ is defined as the difference in χ^2 of a given PV reconstructed with and without the considered track. These $\mu^+\mu^-$ pairs are required to have an invariant mass of less than 5050 MeV/c^2 and to be consistent with originating from a common vertex ($\chi^2_{\rm vtx}$/ndf < 9).

Candidate Λ decays are reconstructed in the $\Lambda \to p\pi^-$ mode from two oppositely-charged particles that either both originate within the acceptance of the VELO ("long Λ" candidates), or both originate outside the acceptance of the VELO ("downstream Λ" candidates). Tracks are required to have $p_{\rm T} > 0.5$ GeV/c, and Λ candidates must have $\chi^2_{\rm vtx}$/ndf < 30 (<25 for downstream Λ candidates), a decay time of at least 2 ps, and a reconstructed invariant mass within 30 MeV/c^2 of the world average value [30]. Due to the distinct kinematics and topology of the Λ decay, it is not necessary to impose particle identification requirements on the decay products of the Λ candidate.

Candidate Λ_b^0 decays are formed by combining Λ and dimuon candidates that originate from a common vertex ($\chi^2_{\rm vtx}$/ndf < 8), have $\chi^2_{\rm IP} < 9$, $\chi^2_{\rm VS} > 100$ and an invariant mass in the interval 4.9–7.0 GeV/c^2. The $\chi^2_{\rm VS}$ is defined as the difference in χ^2 between fits in which the Λ_b^0 decay vertex is assumed to coincide with the PV and allowing the decay vertex to be distinct from the PV. Candidates must also point to the associated PV by requiring the angle between the Λ_b^0 momentum vector and the vector between the PV and the Λ_b^0 decay vertex is less than 8 mrad. The associated PV is the one relative to which the Λ_b^0 candidate has the lowest $\chi^2_{\rm IP}$ value.

The final selection is based on a neural network classifier [31,32] with 15 variables as input. The single most important variable is the χ^2 from a kinematic fit [33] that constrains the decay products of the Λ_b^0, the Λ and the dimuon systems to originate from their respective vertices. Other variables that contribute significantly are the momentum and transverse momentum of the Λ_b^0 candidate, the $\chi^2_{\rm IP}$ and track χ^2/ndf for both muons, the $\chi^2_{\rm IP}$ of the Λ_b^0 candidate, and the separation of the Λ and Λ_b^0 vertices. Downstream and long Λ decays have separate inputs to the neural network for $\chi^2_{\rm IP}$ and $\chi^2_{\rm VS}$ because of the differing track resolution and kinematics. In the final selection of $\Lambda_b^0 \to J/\psi\Lambda$ candidates, the $\mu^+\mu^-$ invariant mass is required to be in the interval 3030–3150 MeV/c^2. The signal sample used to train the neural network consists of simulated $\Lambda_b^0 \to \Lambda\mu^+\mu^-$ events, while background is taken from data in the upper sideband of the Λ_b^0 candidate mass spectrum, between 6.0 and 7.0 GeV/c^2, which is dominated by candidates with dimuon mass in the J/ψ region. The requirement on the output of the neural network is chosen to maximise $N_{\rm S}/\sqrt{N_{\rm S}+N_{\rm B}}$, where $N_{\rm S}$ and $N_{\rm B}$ are the expected numbers of signal and background events, respectively. To ensure an appropriate normalisation of $N_{\rm S}$, the number of $\Lambda_b^0 \to J/\psi\Lambda$ candidates after the preselection is scaled by the measured ratio of branching fractions between the $\Lambda_b^0 \to \Lambda\mu^+\mu^-$ and $\Lambda_b^0 \to J/\psi\Lambda$ decays [16], and the $J/\psi \to \mu^+\mu^-$ branching fraction [30]. The value of $N_{\rm B}$ is derived from the background training sample normalised to the number of candidates in the signal region after preselection. The $\Lambda_b^0 \to \Lambda\mu^+\mu^-$ signal candidates exclude the q^2 regions of 8.68–10.09 GeV/c^4 and 12.86–14.18 GeV/c^4, which are dominated by contributions from the J/ψ and $\psi(2S)$ resonances, respectively. The effect of finite q^2 resolution is negligible. Relative to the preselected event sample, the neural network retains (76.0 ± 0.3)% of the rare decay signal while rejecting (95.9 ± 0.2)% of the background.

4. Peaking backgrounds

Backgrounds are studied using simulated samples of b hadrons in which the final state includes two muons. For the $\Lambda_b^0 \to J/\psi\Lambda$ channel, the only significant contribution found is from $B^0 \to J/\psi K_S^0$ decays, with $K_S^0 \to \pi^+\pi^-$, which has the same topology as the $\Lambda_b^0 \to J/\psi\Lambda$ mode. This contribution leads to a broad shape that peaks below the Λ_b^0 mass region and is accommodated in the mass fit described later.

For the $\Lambda_b^0 \to \Lambda\mu^+\mu^-$ channel, sources of peaking background are considered in the q^2 ranges of interest. The contributions identified are $\Lambda_b^0 \to J/\psi\Lambda$ decays in which an energetic photon is radiated from either of the muons, and $B^0 \to K_S^0\mu^+\mu^-$ decays, where $K_S^0 \to \pi^+\pi^-$ and a pion is misreconstructed as a proton. The $\Lambda_b^0 \to J/\psi\Lambda$ decays contribute in the q^2 region just below $m^2_{J/\psi}$, and populate a mass region significantly below the Λ_b^0 mass. The contribution from the $B^0 \to K_S^0\mu^+\mu^-$ decays is estimated by taking the number of $B^0 \to J/\psi K_S^0$ events found in the $\Lambda_b^0 \to J/\psi\Lambda$ fit, and scaling this by the ratio of world average

branching fractions between the decay processes $B^0 \to K^0_S \mu^+\mu^-$ and $B^0 \to J/\psi K^0_S$ (including the $J/\psi \to \mu^+\mu^-$ branching fraction) [30]. This gives fewer than 10 events integrated over q^2, which is small relative to the expected total background levels.

5. Yields

5.1. Fit description

The yields of signal and background events in the data are determined in the mass range 5.35–5.85 GeV/c^2 using unbinned, extended maximum likelihood fits, for the $\Lambda^0_b \to \Lambda\mu^+\mu^-$ and the $\Lambda^0_b \to J/\psi\Lambda$ modes. The likelihood function has the form

$$\mathcal{L} = e^{-(N_S+N_B+N_P)} \times \prod_{i=1}^{N}\left[N_S P_S(m_i) + N_B P_B(m_i) + N_P P_P(m_i)\right], \quad (1)$$

where N_S, N_B and N_P are number of signal, combinatorial and peaking background events, respectively, and $P_j(m_i)$ are the corresponding probability density functions (PDFs). The mass of the Λ^0_b candidate, m_i, is determined by a kinematic fit of the full decay chain in which the proton and pion are constrained such that the $p\pi^-$ invariant mass corresponds to the Λ baryon mass [30].

The signal shape, in both $\Lambda^0_b \to \Lambda\mu^+\mu^-$ and $\Lambda^0_b \to J/\psi\Lambda$ modes, is described by the sum of two Gaussian functions that share a common mean but have independent widths. The combinatorial background is parametrised by a first-order polynomial, while the background due to $B^0 \to J/\psi K^0_S$ decays is modelled by an exponential function (with a cut-off) convolved with a Gaussian function.

For the $\Lambda^0_b \to J/\psi\Lambda$ mode, the widths and common mean in the signal parametrisation are free parameters. The contribution of the narrower Gaussian function is fixed to be 86% of the total yield based on studies with simulated data. The parameters describing the shape of the peaking background are fixed to those derived from simulated $B^0 \to J/\psi K^0_S$ decays.

For the $\Lambda^0_b \to \Lambda\mu^+\mu^-$ decay, the signal shape parameters are fixed according to the result of the fit to $\Lambda^0_b \to J/\psi\Lambda$ data. Studies with simulated data show that the signal shape parameters in both decay modes are consistent with one another, the only deviations being in the tails of the mass distribution. These are due to small differences in the momentum spectra of the muons and energy loss from radiative effects, and are negligible given the uncertainties inherent in the size of the current data sample. The peaking background is found to be negligible in the q^2 regions considered and is therefore excluded from the fit.

5.2. Fit results

The invariant mass distributions of the $\Lambda^0_b \to J/\psi\Lambda$ candidates is shown in Fig. 1. The fitted function provides a good description of the data, with a χ^2/ndf corresponding to a probability of 47%. The numbers of signal, combinatorial background and peaking background events are found to be 2680 ± 64, 1294 ± 83 and 1501 ± 85, respectively, and the widths of the Gaussian functions are 16.0 ± 0.4 and 33 ± 5 MeV/c^2, compatible with simulation.

The invariant mass distribution for the $\Lambda^0_b \to \Lambda\mu^+\mu^-$ process, integrated over q^2 and in six q^2 intervals, are shown in Figs. 2 and 3, respectively. The yields, both integrated and differential in q^2, are summarised in Table 1. The same q^2 intervals as in Ref. [16] are used to facilitate comparison with the CDF measurements. The statistical significance of the observed signal yields in Table 1 are evaluated as $\sqrt{2\Delta\ln\mathcal{L}}$, where $\Delta\ln\mathcal{L}$ is the change in the logarithm of the likelihood function when the signal component is excluded from the fit, relative to the nominal fit in which it is present. Significant signal yields are only apparent for $q^2 > m^2_{J/\psi}$. Yields at lower-q^2 values are compatible with zero, consistent with previous observations [16].

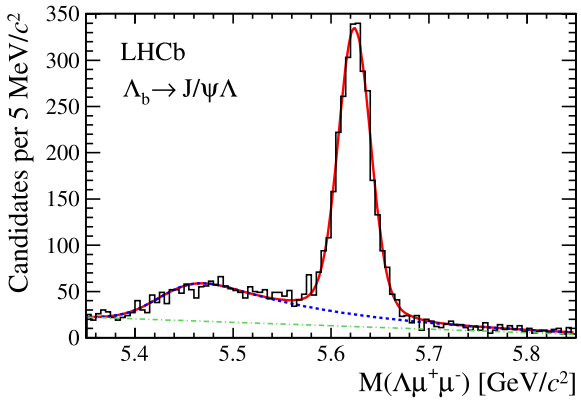

Fig. 1. Invariant mass distribution of the $\Lambda^0_b \to J/\psi\Lambda$ candidates. The histogram shows data, the solid red line is the overall fit function, the dotted blue line represents the sum of the combinatorial and peaking backgrounds and the dash-dotted green line the combinatorial background component. (For interpretation of the references to colour in this figure legend, the reader is referred to the web version of this Letter.)

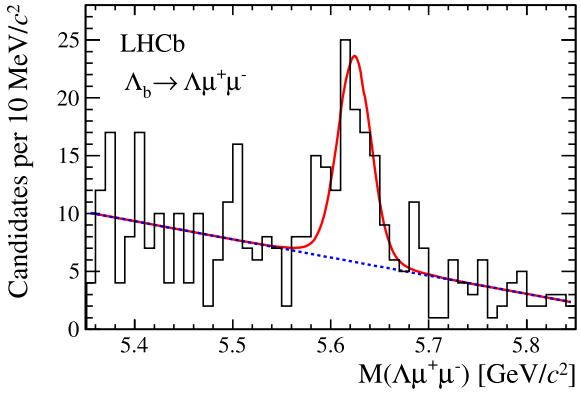

Fig. 2. Invariant mass distribution of the $\Lambda^0_b \to \Lambda\mu^+\mu^-$ candidates, integrated over all q^2 values, together with the fit function described in the text. The histogram shows data, the solid red line is the overall fit function and the dotted blue line represents the background component. (For interpretation of the references to colour in this figure legend, the reader is referred to the web version of this Letter.)

6. Efficiency

The measurement of the differential branching fraction of $\Lambda^0_b \to \Lambda\mu^+\mu^-$ relative to $\Lambda^0_b \to J/\psi\Lambda$ benefits from the cancellation of several potential sources of systematic uncertainty in the ratio of efficiencies, $\varepsilon_{\rm rel} = \varepsilon_{\rm tot}(\Lambda^0_b \to \Lambda\mu^+\mu^-)/\varepsilon_{\rm tot}(\Lambda^0_b \to J/\psi\Lambda)$. The efficiency for each of the decays is calculated according to

$$\varepsilon_{\rm tot} = \varepsilon(\text{geometry})\varepsilon(\text{selection}|\text{geometry}) \times \varepsilon(\text{trigger}|\text{selection}), \quad (2)$$

where the first term represents the efficiency for the final state particles to be within the LHCb angular acceptance, the second term the combined efficiency for candidate detection, reconstruction and selection, and the rightmost term the efficiency for an event to satisfy the trigger requirements if it is reconstructed and selected. All efficiencies are evaluated using simulated data. A phase space model is used for $\Lambda^0_b \to J/\psi\Lambda$ decays. The model

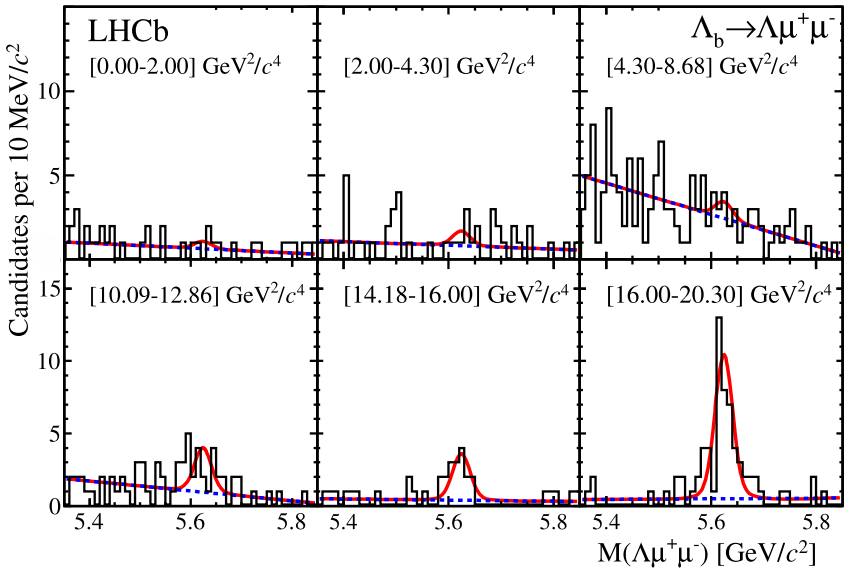

Fig. 3. Invariant mass distributions for the rare decay $\Lambda_b^0 \to \Lambda\mu^+\mu^-$ candidates, in six q^2 intervals, together with the fit function described in the text. The histogram shows data, the solid red line is the overall fit function and the dotted blue line represents the background component. (For interpretation of the references to colour in this figure legend, the reader is referred to the web version of this Letter.)

Table 1
Signal (N_S) and background (N_B) decay yields obtained from the $\Lambda_b^0 \to \Lambda\mu^+\mu^-$ mass fit in each q^2 interval. The integrated yield is the result of a fit without separation of the data into distinct q^2 regions. The statistical significance is calculated as described in the text.

q^2 interval [GeV$^2/c^4$]	N_S	N_B	Significance
0.00–2.00	2 ± 3	34 ± 6	0.8
2.00–4.30	4 ± 3	42 ± 7	1.4
4.30–8.68	4 ± 5	134 ± 12	1.0
10.09–12.86	13 ± 5	52 ± 8	3.4
14.18–16.00	14 ± 4	20 ± 5	4.9
16.00–20.30	44 ± 7	24 ± 6	9.8
Integrated yield	78 ± 12	310 ± 19	8.9

used for $\Lambda_b^0 \to \Lambda\mu^+\mu^-$ decays includes q^2 and angular dependence as described in Ref. [34], together with Wilson coefficients based on Refs. [35,36]. Interference effects from charmonium contributions are not included.

With these models, the geometric acceptance is found to be 16% for $\Lambda_b^0 \to J/\psi\Lambda$ decays and in the range 16–20% (q^2 dependent) for the $\Lambda_b^0 \to \Lambda\mu^+\mu^-$ channel. The overall efficiency to reconstruct and select the $\Lambda_b^0 \to \Lambda\mu^+\mu^-$ decays varies from 1.3% in the lowest q^2 interval to values around 2.5% in the higher-q^2 regions. The $\Lambda_b^0 \to J/\psi\Lambda$ decay has a similar efficiency to the larger-q^2 regions of the rare decay. The trigger efficiency is calculated using an emulation of the hardware trigger, combined with the same software stage of the trigger that was used for data. The trigger efficiency increases from approximately 50% to 80% for the lowest to highest q^2 regions, respectively. An independent cross-check of the trigger efficiency is performed using $\Lambda_b^0 \to J/\psi\Lambda$ data by calculating the ratio of yields that are both classified as trigger on signal and trigger independent of signal relative to those that are only classified as trigger independent of signal. This data-driven method gives an efficiency of $(75 \pm 7)\%$, which is consistent with that of $(70.5 \pm 0.3)\%$ computed from simulation.

The relative efficiency for the ratio of branching fractions in each q^2 interval, calculated from the absolute efficiencies described above, are given in Table 2. The rise in relative efficiency as a function of increasing q^2 is dominated by two effects. Firstly, at low q^2 the muons have lower momenta and therefore have a lower probability of satisfying the trigger requirements. Secondly, at low q^2 the

Table 2
Total relative efficiency, ε_{rel}, between $\Lambda_b^0 \to \Lambda\mu^+\mu^-$ and $\Lambda_b^0 \to J/\psi\Lambda$ decays. The uncertainties are the combination of both statistical and systematic components, and are dominated by the latter.

q^2 interval [GeV$^2/c^4$]	ε_{rel}
0.00–2.00	0.48 ± 0.07
2.00–4.30	0.74 ± 0.08
4.30–8.68	0.88 ± 0.09
10.09–12.86	1.19 ± 0.12
14.18–16.00	1.36 ± 0.14
16.00–20.30	1.28 ± 0.15

Λ baryon has a larger fraction of the Λ_b^0 momentum and is more likely to decay outside of the acceptance. The uncertainties combine both statistical and systematic contributions (with the latter dominating) and include a small correlated uncertainty due to the use of a single sample of $\Lambda_b^0 \to J/\psi\Lambda$ decays as the normalisation channel for all q^2 intervals. The systematic uncertainties are described in more detail in Section 7.

7. Systematic uncertainties

7.1. Yields

Three separate sources of systematic uncertainty on the measured yields are considered for both the $\Lambda_b^0 \to J/\psi\Lambda$ and $\Lambda_b^0 \to \Lambda\mu^+\mu^-$ decay modes: the definition of the signal PDF, the defini-

Table 3
Absolute systematic uncertainties on the yields for the $\Lambda_b^0 \to \Lambda\mu^+\mu^-$ decay.

Source	q^2 interval [GeV$^2/c^4$]					
	0.00–2.00	2.00–4.30	4.30–8.68	10.09–12.86	14.18–16.00	16.00–20.30
Signal PDF	0.08	0.08	0.16	0.4	0.08	2.3
Combinatorial background	2.7	0.7	0.21	3.5	2.2	2.5
Signal shape parameters	0.04	0.08	0.09	0.4	0.17	1.1
Total	2.7	0.7	0.28	3.5	2.2	3.5

tion of the background PDF and the choice of the fixed parameters used in the fits to data.

For the $\Lambda_b^0 \to J/\psi\Lambda$ decays, the default signal PDF is replaced by a single Gaussian function. A 2.0% change in signal yield relative to the default fit is observed and assigned as the systematic uncertainty. The shape of the combinatorial background function is changed from the default first-order polynomial to a second-order polynomial. The 1.8% change in the signal yield is assigned as the systematic uncertainty. To estimate the sensitivity of the background process $B^0 \to J/\psi K_S^0$ to differences between data and simulation, the shape of this background is varied in the fit. A relative uncertainty of 4.7% is assigned. For $\Lambda_b^0 \to \Lambda\mu^+\mu^-$ decays, as the parameter values of the signal PDF are from fits to the $\Lambda_b^0 \to J/\psi\Lambda$ data, the uncertainty in the signal shape is accounted for by using the signal shape parameters and covariance matrix obtained from the $\Lambda_b^0 \to J/\psi\Lambda$ mass fit. The dependence on the shape of the signal PDF is investigated by fitting data using the parameters determined from the single-Gaussian function treatment of the $\Lambda_b^0 \to J/\psi\Lambda$ data described above. The combinatorial background modelling is studied in the same way as for the $\Lambda_b^0 \to J/\psi\Lambda$ decays. The systematic uncertainties on the yield in each q^2 interval are summarised in Table 3, where the total is the sum in quadrature of the three individual components. No additional uncertainty is assigned to account for finite peaking background, as constraining it to the prediction from simulated $B^0 \to K_S^0\mu^+\mu^-$ decays has a negligible effect.

7.2. Relative efficiencies

In measuring the q^2 dependence of the differential branching fraction, three types of correlation are taken into account: those between the normalisation and signal decays; those between the different q^2 regions; and those between the geometric, selection and trigger efficiencies. For simplicity, correlations among q^2 intervals are taken into account where a systematic uncertainty is significant and neglected where a given uncertainty is small compared to the dominant sources. Overall, the dominant systematic effect identified is that related to the current knowledge of the angular structure of the decays and q^2 dependence of the decay channels. The uncertainty due to the finite size of simulated samples used is comparable to that from other sources considered, and is summarised together with all other contributions to the relative efficiency in Table 4, where the total is the sum in quadrature of the individual components.

7.2.1. Decay structure and production polarisation

The main factors that affect the detection efficiencies are the angular structure of the decays and the production polarisation. Although these arise from different parts of the process, the efficiencies are linked and therefore are treated together.

For the $\Lambda_b^0 \to \Lambda\mu^+\mu^-$ decay, the impact of the limited knowledge of the production polarisation, P_b, is estimated by comparing the default efficiency with that in either of the fully polarised scenarios, $P_b = \pm 1$, taking the larger difference as the associated uncertainty. To assess the systematic uncertainty due to the decay structure, the efficiency from the default model [34–36] is compared with that from the phase space decay, taking the larger of this difference or the statistical precision as the systematic uncertainty.

For the $\Lambda_b^0 \to J/\psi\Lambda$ mode, the default phase space decay is compared with the efficiency derived using the model from Ref. [37], which depends on the polarisation parameter P_b and four complex amplitudes. While fixing $P_b = 0$, a scan of the four complex amplitudes is made and the distribution of the change in efficiency relative to the default is constructed. The sum in quadrature of the mean and r.m.s. of this distribution is assigned as the systematic uncertainty due to the decay structure.

To assess the importance of the production polarisation, this exercise is repeated while setting $P_b = \pm 1$. The sum in quadrature of the mean and r.m.s. of the distribution of deviations from the default gives the combined effect of decay structure and production polarisation. The systematic uncertainty due to production polarisation alone is determined by subtracting in quadrature the systematic uncertainty due to the decay structure.

The impact of P_b on the efficiencies is found to be small using the fully polarised scenarios, which are a conservative variation relative to the recent measurement of Ref. [38].

7.2.2. Lifetime of Λ_b^0 baryon

The Λ_b^0 baryon lifetime used throughout is 1.425 ps [30] and the systematic uncertainty associated with this assumption is investigated by varying the lifetime by one standard deviation (0.032 ps). No significant effect is found.

7.2.3. Reconstruction efficiency for Λ baryon

The Λ baryon is reconstructed from either long or downstream tracks, and their relative proportions differ between data and simulation. For simulated $\Lambda_b^0 \to J/\psi\Lambda$ decays, $(21.1 \pm 0.2)\%$ of Λ baryon candidates are reconstructed from long tracks, compared to $(26.4 \pm 0.7)\%$ in data. For the phase space decay distribution of simulated $\Lambda_b^0 \to \Lambda\mu^+\mu^-$ decays, $(21.5 \pm 0.1)\%$ (integrated over q^2) are long tracks, indicating that both decay modes have a similar behaviour. To account for a potential effect due to the different fractions of long and downstream tracks observed in data and simulation, the efficiencies are first determined separately for Λ baryon candidates formed exclusively from long and from downstream tracks. A new relative efficiency is then determined, setting the fraction of downstream tracks to 27% for simulated $\Lambda_b^0 \to J/\psi\Lambda$ decays, and increasing it by 5% in each q^2 interval for simulated $\Lambda_b^0 \to \Lambda\mu^+\mu^-$ decays. The systematic uncertainty from this source is assigned as the difference between this reweighted efficiency and the default case.

7.2.4. Production kinematics

There is a small difference between data and simulation in the momentum and transverse momentum distributions of the Λ baryon produced in the $\Lambda_b^0 \to J/\psi\Lambda$ decays. Simulated data are reweighted to reproduce these distributions in data, and the differences in the relative efficiencies with respect to the default are

Table 4
Absolute systematic uncertainties on the total relative efficiency, $\varepsilon_{\rm rel}$.

Source	q^2 interval [GeV$^2/c^4$]					
	0.00–2.00	2.00–4.30	4.30–8.68	10.09–12.86	14.18–16.00	16.00–20.30
Simulated sample size	0.014	0.015	0.015	0.025	0.04	0.032
Decay structure	0.05	0.07	0.08	0.11	0.13	0.12
Polarisation	0.007	0.007	0.011	0.014	0.015	0.05
Λ reconstruction efficiency	0.027	0.009	0.003	< 0.001	0.003	0.004
Production kinematics	0.023	0.005	0.007	0.026	0.014	0.05
Neural network	0.021	0.027	0.032	0.021	0.002	0.04
Total	0.07	0.08	0.09	0.12	0.14	0.15

Table 5
Measured relative differential branching fraction, $(1/\mathcal{B}(\Lambda_b^0 \to J/\psi\Lambda))\,\mathrm{d}\mathcal{B}(\Lambda_b^0 \to \Lambda\mu^+\mu^-)/\mathrm{d}q^2$. The first uncertainty is statistical and the second is systematic. The systematic uncertainty includes the small, correlated component due to $\mathcal{B}(J/\psi \to \mu^+\mu^-) = (5.93 \pm 0.06) \times 10^{-2}$ [30]. The rightmost column gives the 90% (95%) confidence level upper limit (UL) on the relative branching fraction in q^2 intervals where no significant signal is observed.

q^2 interval [GeV$^2/c^4$]	$\frac{1}{\mathcal{B}(\Lambda_b^0 \to J/\psi\Lambda)}\frac{\mathrm{d}\mathcal{B}}{\mathrm{d}q^2}$ [10^{-4} (GeV$^2/c^4$)$^{-1}$]	UL [10^{-4} (GeV$^2/c^4$)$^{-1}$]
0.00–2.00	$0.45 \pm 0.62 \pm 0.64$	1.7 (2.1)
2.00–4.30	$0.50 \pm 0.41 \pm 0.11$	1.3 (1.5)
4.30–8.68	$0.25 \pm 0.27 \pm 0.03$	0.7 (0.9)
10.09–12.86	$0.90 \pm 0.34 \pm 0.26$	–
14.18–16.00	$1.26 \pm 0.38 \pm 0.25$	–
16.00–20.30	$1.76 \pm 0.29 \pm 0.27$	–

Table 6
Measured differential branching fraction, $\mathrm{d}\mathcal{B}(\Lambda_b^0 \to \Lambda\mu^+\mu^-)/\mathrm{d}q^2$, for $\mathcal{B}(\Lambda_b^0 \to J/\psi\Lambda) = (6.2 \pm 1.4) \times 10^{-4}$ [30], where the first uncertainty is statistical, the second systematic and the third from the uncertainty in $\mathcal{B}(\Lambda_b^0 \to J/\psi\Lambda)$. The rightmost column gives the 90% (95%) confidence level upper limit (UL) on the branching fraction in q^2 intervals where no significant signal is observed.

q^2 interval [GeV$^2/c^4$]	$\mathrm{d}\mathcal{B}/\mathrm{d}q^2$ [10^{-7} (GeV$^2/c^4$)$^{-1}$]	UL [10^{-7} (GeV$^2/c^4$)$^{-1}$]
0.00–2.00	$0.28 \pm 0.38 \pm 0.40 \pm 0.06$	1.2 (1.5)
2.00–4.30	$0.31 \pm 0.26 \pm 0.07 \pm 0.07$	0.9 (1.1)
4.30–8.68	$0.15 \pm 0.17 \pm 0.02 \pm 0.03$	0.5 (0.6)
10.09–12.86	$0.56 \pm 0.21 \pm 0.16 \pm 0.12$	–
14.18–16.00	$0.79 \pm 0.24 \pm 0.15 \pm 0.17$	–
16.00–20.30	$1.10 \pm 0.18 \pm 0.17 \pm 0.24$	–

assigned as the systematic uncertainty due to production kinematics.

7.2.5. Modelling of neural network observables

A discrepancy is observed between data and simulation in the neural network response for $\Lambda_b^0 \to J/\psi\Lambda$ decay candidates. This is due to differences between χ^2 distributions in data and simulation. A systematic uncertainty is assigned as the change relative to the default efficiency after all efficiencies are recalculated using reweighted neural network input variables.

8. Results and conclusion

The relative differential branching fraction is measured in each q^2 interval as

$$\frac{1}{\mathcal{B}(\Lambda_b^0 \to J/\psi\Lambda)}\frac{\mathrm{d}\mathcal{B}(\Lambda_b^0 \to \Lambda\mu^+\mu^-)}{\mathrm{d}q^2} = \frac{N_S(\Lambda_b^0 \to \Lambda\mu^+\mu^-)}{N_S(\Lambda_b^0 \to J/\psi\Lambda)}\frac{1}{\varepsilon_{\rm rel}}\mathcal{B}\big(J/\psi \to \mu^+\mu^-\big)\frac{1}{\Delta q^2}, \quad (3)$$

where Δq^2 represents the width of the given q^2 interval.

For q^2 regions in which no statistically significant signal is observed, an upper limit on $\mathrm{d}\mathcal{B}(\Lambda_b^0 \to \Lambda\mu^+\mu^-)/\mathrm{d}q^2$ is calculated using the following Bayesian approach. The signal PDF for $\Lambda_b^0 \to \Lambda\mu^+\mu^-$ decays is reparametrised in terms of the relative differential rate of Eq. (3), $N_S(\Lambda_b^0 \to J/\psi\Lambda)$, $\varepsilon_{\rm rel}$ and $\mathcal{B}(J/\psi \to \mu^+\mu^-)$. The known uncertainties on the $\Lambda_b^0 \to J/\psi\Lambda$ yield and $\varepsilon_{\rm rel}$ are included in the fit with Gaussian constraints and the profile likelihood over the relative branching fraction is then obtained. An upper limit is set at the value where the posterior likelihood corresponds to 90% (95%). A uniform prior between zero and 3×10^{-3} is used. The limits on the absolute differential branching fractions are given by the product of the relative limit and $\mathcal{B}(\Lambda_b^0 \to J/\psi\Lambda)$ and include the uncertainty on $\mathcal{B}(\Lambda_b^0 \to J/\psi\Lambda)$ from Ref. [30].

The measured relative differential branching fraction is presented in Table 5, while the absolute differential branching fraction is given in Table 6 and shown in Fig. 4. The integrated relative branching fraction is obtained as the sum of the differential rates in six q^2 intervals (weighted by Δq^2). This gives the integral over the full phase space, with the exception of the q^2 regions corresponding to the J/ψ and $\psi(2S)$ resonances. In this integration the statistical uncertainties are added in quadrature. Systematic uncertainties on the $\Lambda_b^0 \to \Lambda\mu^+\mu^-$ yield and the relative efficiency are treated as uncorrelated. The remaining systematic uncertainties, including the statistical and systematic uncertainties in the normalisation mode yield from Ref. [30], are treated as fully correlated. This leads to the relative branching fraction of

$$\frac{\mathcal{B}(\Lambda_b^0 \to \Lambda\mu^+\mu^-)}{\mathcal{B}(\Lambda_b^0 \to J/\psi\Lambda)} = \big(1.54 \pm 0.30(\mathrm{stat}) \pm 0.20(\mathrm{syst}) \pm 0.02(\mathrm{norm})\big) \times 10^{-3},$$

which corresponds to the absolute branching fraction

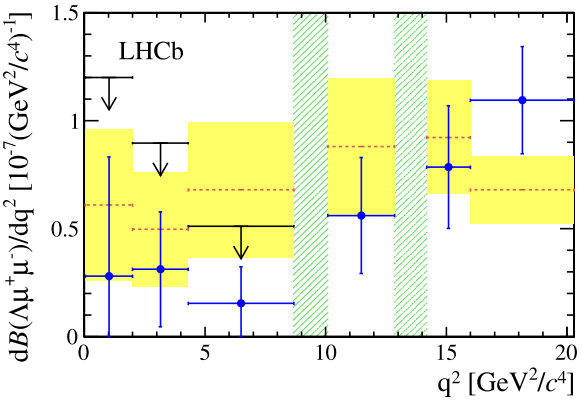

Fig. 4. Measured differential branching fraction for the $\Lambda_b^0 \to \Lambda\mu^+\mu^-$ decay. In regions without a significant signal, the 90% confidence level upper limits are also shown. The uncertainties due to components that are fully correlated across all q^2 bins, e.g. the branching fraction of the normalisation channel from Ref. [30], are not included in this figure. The dashed red line with the filled area shows the theoretical prediction from Ref. [14]. (For interpretation of the references to colour in this figure legend, the reader is referred to the web version of this Letter.)

$$\mathcal{B}\left(\Lambda_b^0 \to \Lambda\mu^+\mu^-\right) = \left(0.96 \pm 0.16(\text{stat}) \pm 0.13(\text{syst}) \pm 0.21(\text{norm})\right) \times 10^{-6},$$

where the last uncertainty accounts for the branching fraction of the normalisation mode [30].

These new measurements of the branching fraction and differential branching fraction for the rare decay $\Lambda_b^0 \to \Lambda\mu^+\mu^-$ are based on a yield of 78 ± 12 signal decays obtained from data, corresponding to an integrated luminosity of 1.0 fb^{-1}, collected at a centre-of-mass energy of 7 TeV. Evidence for this process is found for $q^2 > m^2_{J/\psi}$ and is compatible with previous measurements by the CDF Collaboration [16]. Within the precision of measurements presented in this Letter, the Standard Model predictions of Ref. [14] provide a good description of the data.

Acknowledgements

We express our gratitude to our colleagues in the CERN accelerator departments for the excellent performance of the LHC. We thank the technical and administrative staff at the LHCb institutes. We acknowledge support from CERN and from the national agencies: CAPES, CNPq, FAPERJ and FINEP (Brazil); NSFC (China); CNRS/IN2P3 and Region Auvergne (France); BMBF, DFG, HGF and MPG (Germany); SFI (Ireland); INFN (Italy); FOM and NWO (The Netherlands); SCSR (Poland); ANCS/IFA (Romania); MinES, Rosatom, RFBR and NRC "Kurchatov Institute" (Russia); MinECo, XuntaGal and GENCAT (Spain); SNSF and SER (Switzerland); NAS Ukraine (Ukraine); STFC (United Kingdom); NSF (USA). We also acknowledge the support received from the ERC under FP7. The Tier1 computing centres are supported by IN2P3 (France), KIT and BMBF (Germany), INFN (Italy), NWO and SURF (The Netherlands), PIC (Spain), GridPP (United Kingdom). We are thankful for the computing resources put at our disposal by Yandex LLC (Russia), as well as to the communities behind the multiple open source software packages that we depend on.

Open access

References

[1] T. Mannel, S. Recksiegel, J. Phys. G 24 (1998) 979, arXiv:hep-ph/9701399.
[2] G. Hiller, M. Knecht, F. Legger, T. Schietinger, Phys. Lett. B 649 (2007) 152, arXiv:hep-ph/0702191.
[3] M.J. Aslam, Y.-M. Wang, C.-D. Lu, Phys. Rev. D 78 (2008) 114032, arXiv:0808.2113.
[4] Y.-M. Wang, Y. Li, C.-D. Lu, Eur. Phys. J. C 59 (2009) 861, arXiv:0804.0648.
[5] C.-S. Huang, H.-G. Yan, Phys. Rev. D 59 (1999) 114022, arXiv:hep-ph/9811303.
[6] C.-H. Chen, C.Q. Geng, Phys. Rev. D 63 (2001) 114024, arXiv:hep-ph/0101171.
[7] C.-H. Chen, C.Q. Geng, Phys. Rev. D 64 (2001) 074001, arXiv:hep-ph/0106193.
[8] C.-H. Chen, C.Q. Geng, Phys. Lett. B 516 (2001) 327, arXiv:hep-ph/0101201.
[9] F. Zolfagharpour, V. Bashiry, Nucl. Phys. B 796 (2008) 294, arXiv:0707.4337.
[10] L. Mott, W. Roberts, Int. J. Mod. Phys. A 27 (2012) 1250016, arXiv:1108.6129.
[11] T.M. Aliev, K. Azizi, M. Savci, Phys. Rev. D 81 (2010) 056006, arXiv:1001.0227.
[12] R. Mohanta, A.K. Giri, Phys. Rev. D 82 (2010) 094022, arXiv:1010.1152.
[13] S. Sahoo, C.K. Das, L. Maharana, Int. J. Mod. Phys. A 24 (2009) 6223, arXiv:1112.4563.
[14] W. Detmold, C.-J.D. Lin, S. Meinel, M. Wingate, Phys. Rev. D 87 (2013) 074502, arXiv:1212.4827.
[15] T. Gutsche, et al., Phys. Rev. D 87 (2013) 074031, arXiv:1301.3737.
[16] CDF Collaboration, T. Aaltonen, et al., Phys. Rev. Lett. 107 (2011) 201802, arXiv:1107.3753.
[17] LHCb Collaboration, R. Aaij, et al., JHEP 1301 (2013) 90, arXiv:1209.4029.
[18] LHCb Collaboration, R. Aaij, et al., Differential branching fraction and angular analysis of the decay $B_s^0 \to \phi\mu^+\mu^-$, arXiv:1305.2168, JHEP (2013), in press.
[19] LHCb Collaboration, A.A. Alves Jr., et al., JINST 3 (2008) S08005.
[20] M. Adinolfi, et al., Eur. Phys. J. C 73 (2013) 2431, arXiv:1211.6759.
[21] A.A. Alves Jr., et al., JINST 8 (2013) P02022, arXiv:1211.1346.
[22] R. Aaij, et al., JINST 8 (2013) P04022, arXiv:1211.3055.
[23] T. Sjöstrand, S. Mrenna, P. Skands, JHEP 0605 (2006) 026, arXiv:hep-ph/0603175.
[24] I. Belyaev, et al., Nuclear Science Symposium Conference Record (NSS/MIC), IEEE (2010) 1155.
[25] D.J. Lange, Nucl. Instrum. Meth. A 462 (2001) 152.
[26] P. Golonka, Z. Was, Eur. Phys. J. C 45 (2006) 97, arXiv:hep-ph/0506026.
[27] GEANT4 Collaboration, J. Allison, et al., IEEE Trans. Nucl. Sci. 53 (2006) 270.
[28] GEANT4 Collaboration, S. Agostinelli, et al., Nucl. Instrum. Meth. A 506 (2003) 250.
[29] M. Clemencic, et al., J. Phys.: Conf. Ser. 331 (2011) 032023.
[30] Particle Data Group, J. Beringer, et al., Review of particle physics, Phys. Rev. D 86 (2012) 010001.
[31] M. Feindt, U. Kerzel, Nucl. Instrum. Meth. A 559 (2006) 190.
[32] M. Feindt, arXiv:physics/0402093.
[33] W.D. Hulsbergen, Nucl. Instrum. Meth. A 552 (2005) 566, arXiv:physics/0503191.
[34] T.M. Aliev, M. Savci, JHEP 0605 (2006) 001, arXiv:hep-ph/0507324.
[35] A.J. Buras, M. Munz, Phys. Rev. D 52 (1995) 186, arXiv:hep-ph/9501281.
[36] A.J. Buras, M. Misiak, M. Munz, S. Pokorski, Nucl. Phys. B 424 (1994) 374, arXiv:hep-ph/9311345.
[37] J. Hrivnac, R. Lednicky, M. Smizanska, J. Phys. G 21 (1995) 629, arXiv:hep-ph/9405231.
[38] LHCb Collaboration, R. Aaij, et al., Phys. Lett. B 724 (2013) 27, arXiv:1302.5578.

LHCb Collaboration

R. Aaij [40], B. Adeva [36], M. Adinolfi [45], C. Adrover [6], A. Affolder [51], Z. Ajaltouni [5], J. Albrecht [9], F. Alessio [37], M. Alexander [50], S. Ali [40], G. Alkhazov [29], P. Alvarez Cartelle [36], A.A. Alves Jr. [24,37], S. Amato [2], S. Amerio [21], Y. Amhis [7], L. Anderlini [17,f], J. Anderson [39], R. Andreassen [56], J.E. Andrews [57], R.B. Appleby [53], O. Aquines Gutierrez [10], F. Archilli [18],

A. Artamonov [34], M. Artuso [58], E. Aslanides [6], G. Auriemma [24,m], M. Baalouch [5], S. Bachmann [11], J.J. Back [47], C. Baesso [59], V. Balagura [30], W. Baldini [16], R.J. Barlow [53], C. Barschel [37], S. Barsuk [7], W. Barter [46], Th. Bauer [40], A. Bay [38], J. Beddow [50], F. Bedeschi [22], I. Bediaga [1], S. Belogurov [30], K. Belous [34], I. Belyaev [30], E. Ben-Haim [8], G. Bencivenni [18], S. Benson [49], J. Benton [45], A. Berezhnoy [31], R. Bernet [39], M.-O. Bettler [46], M. van Beuzekom [40], A. Bien [11], S. Bifani [44], T. Bird [53], A. Bizzeti [17,h], P.M. Bjørnstad [53], T. Blake [37], F. Blanc [38], J. Blouw [11], S. Blusk [58], V. Bocci [24], A. Bondar [33], N. Bondar [29], W. Bonivento [15], S. Borghi [53], A. Borgia [58], T.J.V. Bowcock [51], E. Bowen [39], C. Bozzi [16], T. Brambach [9], J. van den Brand [41], J. Bressieux [38], D. Brett [53], M. Britsch [10], T. Britton [58], N.H. Brook [45], H. Brown [51], I. Burducea [28], A. Bursche [39], G. Busetto [21,q], J. Buytaert [37], S. Cadeddu [15], O. Callot [7], M. Calvi [20,j], M. Calvo Gomez [35,n], A. Camboni [35], P. Campana [18,37], D. Campora Perez [37], A. Carbone [14,c], G. Carboni [23,k], R. Cardinale [19,i], A. Cardini [15], H. Carranza-Mejia [49], L. Carson [52], K. Carvalho Akiba [2], G. Casse [51], L. Castillo Garcia [37], M. Cattaneo [37], Ch. Cauet [9], R. Cenci [57], M. Charles [54], Ph. Charpentier [37], P. Chen [3,38], N. Chiapolini [39], M. Chrzaszcz [25], K. Ciba [37], X. Cid Vidal [37], G. Ciezarek [52], P.E.L. Clarke [49], M. Clemencic [37], H.V. Cliff [46], J. Closier [37], C. Coca [28], V. Coco [40], J. Cogan [6], E. Cogneras [5], P. Collins [37], A. Comerma-Montells [35], A. Contu [15,37], A. Cook [45], M. Coombes [45], S. Coquereau [8], G. Corti [37], B. Couturier [37], G.A. Cowan [49], D.C. Craik [47], S. Cunliffe [52], R. Currie [49], C. D'Ambrosio [37], P. David [8], P.N.Y. David [40], A. Davis [56], I. De Bonis [4], K. De Bruyn [40], S. De Capua [53], M. De Cian [39], J.M. De Miranda [1], L. De Paula [2], W. De Silva [56], P. De Simone [18], D. Decamp [4], M. Deckenhoff [9], L. Del Buono [8], N. Déléage [4], D. Derkach [54], O. Deschamps [5], F. Dettori [41], A. Di Canto [11], F. Di Ruscio [23,k], H. Dijkstra [37], M. Dogaru [28], S. Donleavy [51], F. Dordei [11], A. Dosil Suárez [36], D. Dossett [47], A. Dovbnya [42], F. Dupertuis [38], P. Durante [37], R. Dzhelyadin [34], A. Dziurda [25], A. Dzyuba [29], S. Easo [48,37], U. Egede [52], V. Egorychev [30], S. Eidelman [33], D. van Eijk [40], S. Eisenhardt [49], U. Eitschberger [9], R. Ekelhof [9], L. Eklund [50,37], I. El Rifai [5], Ch. Elsasser [39], A. Falabella [14,e], C. Färber [11], G. Fardell [49], C. Farinelli [40], S. Farry [51], V. Fave [38], D. Ferguson [49], V. Fernandez Albor [36], F. Ferreira Rodrigues [1], M. Ferro-Luzzi [37], S. Filippov [32], M. Fiore [16], C. Fitzpatrick [37], M. Fontana [10], F. Fontanelli [19,i], R. Forty [37], O. Francisco [2], M. Frank [37], C. Frei [37], M. Frosini [17,f], S. Furcas [20], E. Furfaro [23,k], A. Gallas Torreira [36], D. Galli [14,c], M. Gandelman [2], P. Gandini [58], Y. Gao [3], J. Garofoli [58], P. Garosi [53], J. Garra Tico [46], L. Garrido [35], C. Gaspar [37], R. Gauld [54], E. Gersabeck [11], M. Gersabeck [53], T. Gershon [47,37], Ph. Ghez [4], V. Gibson [46], L. Giubega [28], V.V. Gligorov [37], C. Göbel [59], D. Golubkov [30], A. Golutvin [52,30,37], A. Gomes [2], H. Gordon [54], M. Grabalosa Gándara [5], R. Graciani Diaz [35], L.A. Granado Cardoso [37], E. Graugés [35], G. Graziani [17], A. Grecu [28], E. Greening [54], S. Gregson [46], P. Griffith [44], O. Grünberg [60], B. Gui [58], E. Gushchin [32], Yu. Guz [34,37], T. Gys [37], C. Hadjivasiliou [58], G. Haefeli [38], C. Haen [37], S.C. Haines [46], S. Hall [52], B. Hamilton [57], T. Hampson [45], S. Hansmann-Menzemer [11], N. Harnew [54], S.T. Harnew [45], J. Harrison [53], T. Hartmann [60], J. He [37], T. Head [37], V. Heijne [40], K. Hennessy [51], P. Henrard [5], J.A. Hernando Morata [36], E. van Herwijnen [37], A. Hicheur [1], E. Hicks [51], D. Hill [54], M. Hoballah [5], M. Holtrop [40], C. Hombach [53], P. Hopchev [4], W. Hulsbergen [40], P. Hunt [54], T. Huse [51], N. Hussain [54], D. Hutchcroft [51], D. Hynds [50], V. Iakovenko [43], M. Idzik [26], P. Ilten [12], R. Jacobsson [37], A. Jaeger [11], E. Jans [40], P. Jaton [38], A. Jawahery [57], F. Jing [3], M. John [54], D. Johnson [54], C.R. Jones [46], C. Joram [37], B. Jost [37], M. Kaballo [9], S. Kandybei [42], W. Kanso [6], M. Karacson [37], T.M. Karbach [37], I.R. Kenyon [44], T. Ketel [41], A. Keune [38], B. Khanji [20], O. Kochebina [7], I. Komarov [38], R.F. Koopman [41], P. Koppenburg [40], M. Korolev [31], A. Kozlinskiy [40], L. Kravchuk [32], K. Kreplin [11], M. Kreps [47,*], G. Krocker [11], P. Krokovny [33], F. Kruse [9], M. Kucharczyk [20,25,j], V. Kudryavtsev [33], T. Kvaratskheliya [30,37], V.N. La Thi [38], D. Lacarrere [37], G. Lafferty [53], A. Lai [15], D. Lambert [49], R.W. Lambert [41], E. Lanciotti [37], G. Lanfranchi [18], C. Langenbruch [37], T. Latham [47], C. Lazzeroni [44], R. Le Gac [6], J. van Leerdam [40], J.-P. Lees [4], R. Lefèvre [5], A. Leflat [31], J. Lefrançois [7], S. Leo [22], O. Leroy [6], T. Lesiak [25], B. Leverington [11], Y. Li [3], L. Li Gioi [5], M. Liles [51], R. Lindner [37], C. Linn [11],

B. Liu [3], G. Liu [37], S. Lohn [37], I. Longstaff [50], J.H. Lopes [2], N. Lopez-March [38], H. Lu [3], D. Lucchesi [21,q], J. Luisier [38], H. Luo [49], F. Machefert [7], I.V. Machikhiliyan [4,30], F. Maciuc [28], O. Maev [29,37], S. Malde [54], G. Manca [15,d], G. Mancinelli [6], J. Maratas [5], U. Marconi [14], P. Marino [22,s], R. Märki [38], J. Marks [11], G. Martellotti [24], A. Martens [8], A. Martín Sánchez [7], M. Martinelli [40], D. Martinez Santos [41], D. Martins Tostes [2], A. Massafferri [1], R. Matev [37], Z. Mathe [37], C. Matteuzzi [20], E. Maurice [6], A. Mazurov [16,32,37,e], B. Mc Skelly [51], J. McCarthy [44], A. McNab [53], R. McNulty [12], B. Meadows [56,54], F. Meier [9], M. Meissner [11], M. Merk [40], D.A. Milanes [8], M.-N. Minard [4], J. Molina Rodriguez [59], S. Monteil [5], D. Moran [53], P. Morawski [25], A. Mordà [6], M.J. Morello [22,s], R. Mountain [58], I. Mous [40], F. Muheim [49], K. Müller [39], R. Muresan [28], B. Muryn [26], B. Muster [38], P. Naik [45], T. Nakada [38], R. Nandakumar [48], I. Nasteva [1], M. Needham [49], S. Neubert [37], N. Neufeld [37], A.D. Nguyen [38], T.D. Nguyen [38], C. Nguyen-Mau [38,o], M. Nicol [7], V. Niess [5], R. Niet [9], N. Nikitin [31], T. Nikodem [11], A. Nomerotski [54], A. Novoselov [34], A. Oblakowska-Mucha [26], V. Obraztsov [34], S. Oggero [40], S. Ogilvy [50], O. Okhrimenko [43], R. Oldeman [15,d], M. Orlandea [28], J.M. Otalora Goicochea [2], P. Owen [52], A. Oyanguren [35], B.K. Pal [58], A. Palano [13,b], M. Palutan [18], J. Panman [37], A. Papanestis [48], M. Pappagallo [50], C. Parkes [53], C.J. Parkinson [52], G. Passaleva [17], G.D. Patel [51], M. Patel [52], G.N. Patrick [48], C. Patrignani [19,i], C. Pavel-Nicorescu [28], A. Pazos Alvarez [36], A. Pellegrino [40], G. Penso [24,l], M. Pepe Altarelli [37], S. Perazzini [14,c], E. Perez Trigo [36], A. Pérez-Calero Yzquierdo [35], P. Perret [5], M. Perrin-Terrin [6], L. Pescatore [44], G. Pessina [20], K. Petridis [52], A. Petrolini [19,i], A. Phan [58], E. Picatoste Olloqui [35], B. Pietrzyk [4], T. Pilař [47], D. Pinci [24], S. Playfer [49], M. Plo Casasus [36], F. Polci [8], G. Polok [25], A. Poluektov [47,33], E. Polycarpo [2], A. Popov [34], D. Popov [10], B. Popovici [28], C. Potterat [35], A. Powell [54], J. Prisciandaro [38], A. Pritchard [51], C. Prouve [7], V. Pugatch [43], A. Puig Navarro [38], G. Punzi [22,r], W. Qian [4], J.H. Rademacker [45], B. Rakotomiaramanana [38], M.S. Rangel [2], I. Raniuk [42], N. Rauschmayr [37], G. Raven [41], S. Redford [54], M.M. Reid [47], A.C. dos Reis [1], S. Ricciardi [48], A. Richards [52], K. Rinnert [51], V. Rives Molina [35], D.A. Roa Romero [5], P. Robbe [7], D.A. Roberts [57], E. Rodrigues [53], P. Rodriguez Perez [36], S. Roiser [37], V. Romanovsky [34], A. Romero Vidal [36], J. Rouvinet [38], T. Ruf [37], F. Ruffini [22], H. Ruiz [35], P. Ruiz Valls [35], G. Sabatino [24,k], J.J. Saborido Silva [36], N. Sagidova [29], P. Sail [50], B. Saitta [15,d], V. Salustino Guimaraes [2], C. Salzmann [39], B. Sanmartin Sedes [36], M. Sannino [19,i], R. Santacesaria [24], C. Santamarina Rios [36], E. Santovetti [23,k], M. Sapunov [6], A. Sarti [18,l], C. Satriano [24,m], A. Satta [23], M. Savrie [16,e], D. Savrina [30,31], P. Schaack [52], M. Schiller [41], H. Schindler [37], M. Schlupp [9], M. Schmelling [10], B. Schmidt [37], O. Schneider [38], A. Schopper [37], M.-H. Schune [7], R. Schwemmer [37], B. Sciascia [18], A. Sciubba [24], M. Seco [36], A. Semennikov [30], I. Sepp [52], N. Serra [39], J. Serrano [6], P. Seyfert [11], M. Shapkin [34], I. Shapoval [16,42], P. Shatalov [30], Y. Shcheglov [29], T. Shears [51,37], L. Shekhtman [33], O. Shevchenko [42], V. Shevchenko [30], A. Shires [52], R. Silva Coutinho [47], M. Sirendi [46], T. Skwarnicki [58], N.A. Smith [51], E. Smith [54,48], J. Smith [46], M. Smith [53], M.D. Sokoloff [56], F.J.P. Soler [50], F. Soomro [18], D. Souza [45], B. Souza De Paula [2], B. Spaan [9], A. Sparkes [49], P. Spradlin [50], F. Stagni [37], S. Stahl [11], O. Steinkamp [39], S. Stoica [28], S. Stone [58], B. Storaci [39], M. Straticiuc [28], U. Straumann [39], V.K. Subbiah [37], L. Sun [56], S. Swientek [9], V. Syropoulos [41], M. Szczekowski [27], P. Szczypka [38,37], T. Szumlak [26], S. T'Jampens [4], M. Teklishyn [7], E. Teodorescu [28], F. Teubert [37], C. Thomas [54], E. Thomas [37], J. van Tilburg [11], V. Tisserand [4], M. Tobin [38], S. Tolk [41], D. Tonelli [37], S. Topp-Joergensen [54], N. Torr [54], E. Tournefier [4,52], S. Tourneur [38], M.T. Tran [38], M. Tresch [39], A. Tsaregorodtsev [6], P. Tsopelas [40], N. Tuning [40], M. Ubeda Garcia [37], A. Ukleja [27], D. Urner [53], A. Ustyuzhanin [52,p], U. Uwer [11], V. Vagnoni [14], G. Valenti [14], A. Vallier [7], M. Van Dijk [45], R. Vazquez Gomez [18], P. Vazquez Regueiro [36], C. Vázquez Sierra [36], S. Vecchi [16], J.J. Velthuis [45], M. Veltri [17,g], G. Veneziano [38], M. Vesterinen [37], B. Viaud [7], D. Vieira [2], X. Vilasis-Cardona [35,n], A. Vollhardt [39], D. Volyanskyy [10], D. Voong [45], A. Vorobyev [29], V. Vorobyev [33], C. Voß [60], H. Voss [10], R. Waldi [60], C. Wallace [47], R. Wallace [12], S. Wandernoth [11], J. Wang [58], D.R. Ward [46],

N.K. Watson [44], A.D. Webber [53], D. Websdale [52], M. Whitehead [47], J. Wicht [37], J. Wiechczynski [25], D. Wiedner [11], L. Wiggers [40], G. Wilkinson [54], M.P. Williams [47,48], M. Williams [55], F.F. Wilson [48], J. Wimberley [57], J. Wishahi [9], M. Witek [25], S.A. Wotton [46], S. Wright [46], S. Wu [3], K. Wyllie [37], Y. Xie [49,37], Z. Xing [58], Z. Yang [3], R. Young [49], X. Yuan [3], O. Yushchenko [34], M. Zangoli [14], M. Zavertyaev [10,a], F. Zhang [3], L. Zhang [58], W.C. Zhang [12], Y. Zhang [3], A. Zhelezov [11], A. Zhokhov [30], L. Zhong [3], A. Zvyagin [37]

[1] Centro Brasileiro de Pesquisas Físicas (CBPF), Rio de Janeiro, Brazil
[2] Universidade Federal do Rio de Janeiro (UFRJ), Rio de Janeiro, Brazil
[3] Center for High Energy Physics, Tsinghua University, Beijing, China
[4] LAPP, Université de Savoie, CNRS/IN2P3, Annecy-Le-Vieux, France
[5] Clermont Université, Université Blaise Pascal, CNRS/IN2P3, LPC, Clermont-Ferrand, France
[6] CPPM, Aix-Marseille Université, CNRS/IN2P3, Marseille, France
[7] LAL, Université Paris-Sud, CNRS/IN2P3, Orsay, France
[8] LPNHE, Université Pierre et Marie Curie, Université Paris Diderot, CNRS/IN2P3, Paris, France
[9] Fakultät Physik, Technische Universität Dortmund, Dortmund, Germany
[10] Max-Planck-Institut für Kernphysik (MPIK), Heidelberg, Germany
[11] Physikalisches Institut, Ruprecht-Karls-Universität Heidelberg, Heidelberg, Germany
[12] School of Physics, University College Dublin, Dublin, Ireland
[13] Sezione INFN di Bari, Bari, Italy
[14] Sezione INFN di Bologna, Bologna, Italy
[15] Sezione INFN di Cagliari, Cagliari, Italy
[16] Sezione INFN di Ferrara, Ferrara, Italy
[17] Sezione INFN di Firenze, Firenze, Italy
[18] Laboratori Nazionali dell'INFN di Frascati, Frascati, Italy
[19] Sezione INFN di Genova, Genova, Italy
[20] Sezione INFN di Milano Bicocca, Milano, Italy
[21] Sezione INFN di Padova, Padova, Italy
[22] Sezione INFN di Pisa, Pisa, Italy
[23] Sezione INFN di Roma Tor Vergata, Roma, Italy
[24] Sezione INFN di Roma La Sapienza, Roma, Italy
[25] Henryk Niewodniczanski Institute of Nuclear Physics Polish Academy of Sciences, Kraków, Poland
[26] AGH – University of Science and Technology, Faculty of Physics and Applied Computer Science, Kraków, Poland
[27] National Center for Nuclear Research (NCBJ), Warsaw, Poland
[28] Horia Hulubei National Institute of Physics and Nuclear Engineering, Bucharest-Magurele, Romania
[29] Petersburg Nuclear Physics Institute (PNPI), Gatchina, Russia
[30] Institute of Theoretical and Experimental Physics (ITEP), Moscow, Russia
[31] Institute of Nuclear Physics, Moscow State University (SINP MSU), Moscow, Russia
[32] Institute for Nuclear Research of the Russian Academy of Sciences (INR RAN), Moscow, Russia
[33] Budker Institute of Nuclear Physics (SB RAS) and Novosibirsk State University, Novosibirsk, Russia
[34] Institute for High Energy Physics (IHEP), Protvino, Russia
[35] Universitat de Barcelona, Barcelona, Spain
[36] Universidad de Santiago de Compostela, Santiago de Compostela, Spain
[37] European Organization for Nuclear Research (CERN), Geneva, Switzerland
[38] Ecole Polytechnique Fédérale de Lausanne (EPFL), Lausanne, Switzerland
[39] Physik-Institut, Universität Zürich, Zürich, Switzerland
[40] Nikhef National Institute for Subatomic Physics, Amsterdam, The Netherlands
[41] Nikhef National Institute for Subatomic Physics and VU University Amsterdam, Amsterdam, The Netherlands
[42] NSC Kharkiv Institute of Physics and Technology (NSC KIPT), Kharkiv, Ukraine
[43] Institute for Nuclear Research of the National Academy of Sciences (KINR), Kyiv, Ukraine
[44] University of Birmingham, Birmingham, United Kingdom
[45] H.H. Wills Physics Laboratory, University of Bristol, Bristol, United Kingdom
[46] Cavendish Laboratory, University of Cambridge, Cambridge, United Kingdom
[47] Department of Physics, University of Warwick, Coventry, United Kingdom
[48] STFC Rutherford Appleton Laboratory, Didcot, United Kingdom
[49] School of Physics and Astronomy, University of Edinburgh, Edinburgh, United Kingdom
[50] School of Physics and Astronomy, University of Glasgow, Glasgow, United Kingdom
[51] Oliver Lodge Laboratory, University of Liverpool, Liverpool, United Kingdom
[52] Imperial College London, London, United Kingdom
[53] School of Physics and Astronomy, University of Manchester, Manchester, United Kingdom
[54] Department of Physics, University of Oxford, Oxford, United Kingdom
[55] Massachusetts Institute of Technology, Cambridge, MA, United States
[56] University of Cincinnati, Cincinnati, OH, United States
[57] University of Maryland, College Park, MD, United States
[58] Syracuse University, Syracuse, NY, United States
[59] Pontifícia Universidade Católica do Rio de Janeiro (PUC-Rio), Rio de Janeiro, Brazil [t]
[60] Institut für Physik, Universität Rostock, Rostock, Germany [u]

* Corresponding author.
E-mail address: M.Kreps@warwick.ac.uk (M. Kreps).
[a] P.N. Lebedev Physical Institute, Russian Academy of Science (LPI RAS), Moscow, Russia.
[b] Università di Bari, Bari, Italy.
[c] Università di Bologna, Bologna, Italy.
[d] Università di Cagliari, Cagliari, Italy.
[e] Università di Ferrara, Ferrara, Italy.

[f] Università di Firenze, Firenze, Italy.
[g] Università di Urbino, Urbino, Italy.
[h] Università di Modena e Reggio Emilia, Modena, Italy.
[i] Università di Genova, Genova, Italy.
[j] Università di Milano Bicocca, Milano, Italy.
[k] Università di Roma Tor Vergata, Roma, Italy.
[l] Università di Roma La Sapienza, Roma, Italy.
[m] Università della Basilicata, Potenza, Italy.
[n] LIFAELS, La Salle, Universitat Ramon Llull, Barcelona, Spain.
[o] Hanoi University of Science, Hanoi, Viet Nam.
[p] Institute of Physics and Technology, Moscow, Russia.
[q] Università di Padova, Padova, Italy.
[r] Università di Pisa, Pisa, Italy.
[s] Scuola Normale Superiore, Pisa, Italy.
[t] Associated to: Universidade Federal do Rio de Janeiro (UFRJ), Rio de Janeiro, Brazil.
[u] Associated to: Physikalisches Institut, Ruprecht-Karls-Universität Heidelberg, Heidelberg, Germany.